Supplementary Information for

Synthesis of Metal-Free Lightweight Materials with Sequence-Encoded Properties

Adi Azoulay[a], Jesús Barrio[a], Jonathan Tzadikov[a], Michael Volokh[a], Josep Albero[b], Christel Gervais[c], Pilar Amo-Ochoa[d], Hermenegildo García[b], Félix Zamora[d,e], Menny Shalom[a]*

a. Department of Chemistry and Ilse Katz Institute for Nanoscale Science and Technology, Ben-Gurion University of the Negev, Beer-Sheva 8410501, Israel. E-mail: mennysh@bgu.ac.il

b. Instituto Universitario Mixto de Tecnología Química (UPV-CSIC), Universitat Politècnica de València, Avda. de los Narajos s/n, 46022, Valencia, Spain.

c. Sorbonne Université, College de France, Laboratoire de Chimie de la Matière Condensée de Paris (LCMCP), UMR CNRS 7574 4 place Jussieu, 75252 Paris cedex 05, France.

d. Departamento de Química Inorgánica, Institute for Advanced Research in Chemical Sciences (IAdChem) and Condensed Matter Physics Center (IFIMAC). Universidad Autónoma de Madrid, E-28049 Madrid, Spain.

e. Instituto Madrileño de Estudios Avanzados en Nanociencia (IMDEA-Nanociencia). Cantoblanco E-28049 Madrid, Spain.

Table S1. Crystal structure parameters of bis(2,4,6-triamino-1,3,5-triazin-1-ium) hydrogen phosphate trihydrate, 2,4,6-triamino-1,3,5-triazinium orthophosphate and 2,4,6-triamino-*s*-triazine.

	PA_2M_1 [1] 2,4,6-triamino-1,3,5-triazinium orthophosphate	**PA_1M_2** [2,3] bis(2,4,6-triamino-1,3,5-triazin-1-ium) hydrogen phosphate trihydrate	**PA_1M_4** [4] 2,4,6-triamino-*s*-triazine
Temperature (K)	296	296	296
Empirical formula	$C_3H_9N_6O_4P$	$C_6H_{21}N_{12}O_7P$	$C_3H_5N_6$
Space group	*P*-1	*P*-1	$P2_1/n$
Crystal system	Triclinic	Triclinic	Monoclinic
***a* (Å)**	4.58	6.81	7.29
***b* (Å)**	9.37	10.58	7.49
***c* (Å)**	10.24	12.52	10.40
***α* (°)**	83.42	91.80	90
***β* (°)**	88.24	105.65	108.43
***γ* (°)**	85.38	108.11	90

Table S2. Single-crystal X-ray CIF data of new PA_1M_1 crystal.

	PA_1M_1
Temperature (K)	293
Empirical formula	$C_3H_{12}N_6O_8P_2$
***M* /g mol $^{-1}$**	322.13
Space group	*P2/c*
Crystal size/mm	0.1 × 0.1 × 0.1
Crystal System	Monoclinic
***a* (Å)**	4.57630(10)
***b* (Å)**	8.0571(2)
***c* (Å)**	16.5465(4)
***α* (°)**	90
***β* (°)**	95.331(2)
***γ* (°)**	90
***V* (Å^3)**	607.46(2)
Z	2
***ρ* (g cm^{-3})**	1.761
***μ* (mm^{-1})**	3.789
***F*(000)**	332.0
Ab. correct.	multi-scan
T_{min}/ T_{max}	0.719/ 0.685
$2\Theta_{max}$	136.736
Total reflns.	2147
Unique reflns.	1113
Obs. reflns.	1034
R_{int}	0.0504
Radiation	CuKα
Wavelength (Å)	1.54184
***hkl* range**	$-5 \le h \le 5$
	$-9 \le k \le 9$
	$-1 \le l \le 19$
No. of reflections	1113

No. of parameters	115
R1 [I> 2σ(I)]	0.0487
wR2 [I> 2σ(I)]	0.1273
R1[all data]	0.0505
wR2 [all data]	0.1293
Goodness of fit	1.113
$\Delta\rho_{max}$, $\Delta\rho_{min}$(eÅ^{-3})	0.51, –0.31
CCDC no.	1923238

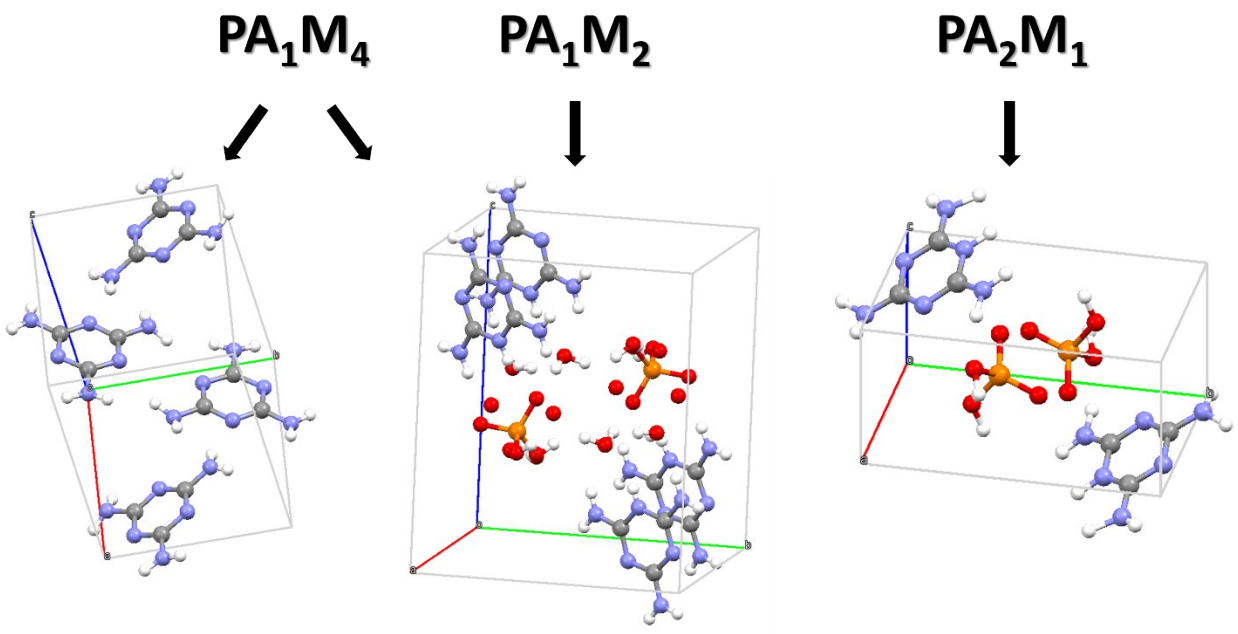

Fig. S1 PA_xM_y single crystal packing structures. In all three cells the orientation is as follows: "a" axis is marked in red, "b" axis is marked in green, and "c" axis is marked in blue.

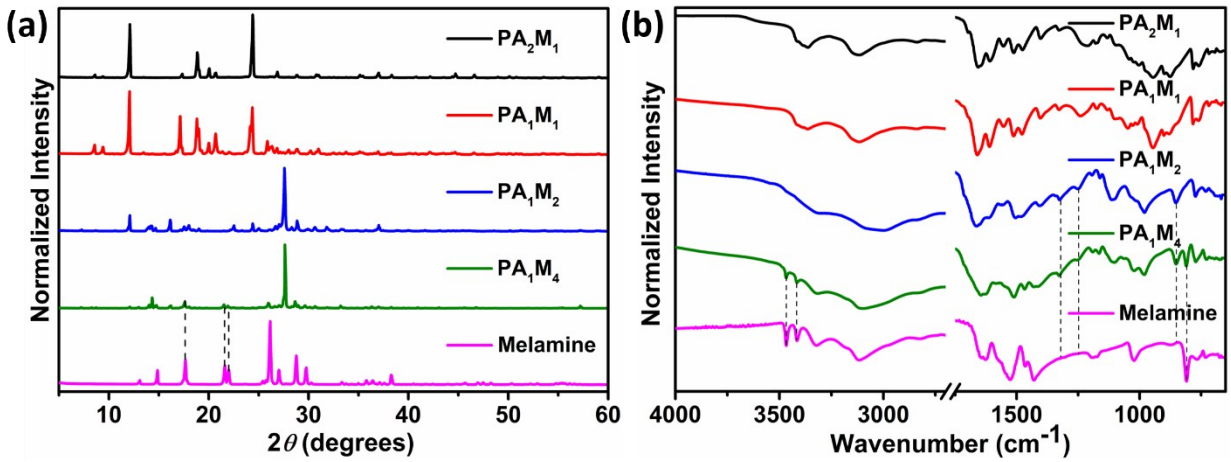

Fig. S2 Melamine and PA_xM_y (a) XRD patterns and (b) FTIR spectra. Patterns and spectra are offset for clarity.

XRD patterns of PA_1M_4, match almost perfectly with PA_1M_2 except its pattern shows low intense peaks at 17.7°, 21.6°, and 22° corresponding to the remaining non-reacting melamine units, further confirming PA_1M_2 and M superposition. FTIR spectroscopy measurements of the prepared crystals further confirm the establishment of an arrangement between phosphoric acid and melamine, as shown by the disappearance of the –NH stretching vibration of the amine groups within melamine units at 3468 and 3416 cm^{-1} as the amine hydrogen is connected either to another melamine (M) unit or PA. These vibrations are still present in PA_1M_4, further supporting the existence of non-reacting melamine units within the crystal. Another peak, located at 810 cm^{-1}, which correspond to the out-of-plane bending of melamine cyclic ring, also confirms the existence of the insulated melamine units. Moreover, two other peaks appear at 1250 (P=O) and 1324 cm^{-1} (P-O-C), provide an evidence for the existence of PA_1M_2 single-crystal in the mixture, indicating a superposition of two different single crystals as well.

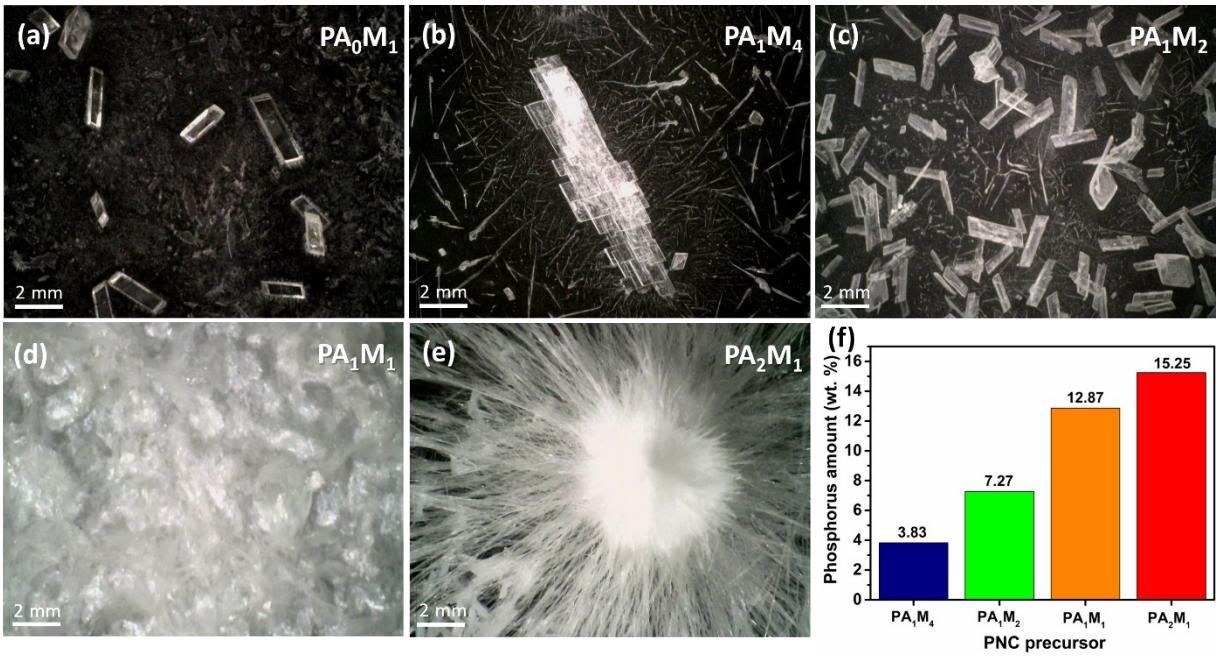

Fig. S3 (a–e) Optical microscopy images of PA_xM_y crystals, and (f) their phosphorus content in weight percentage, determined by ICP-OES.

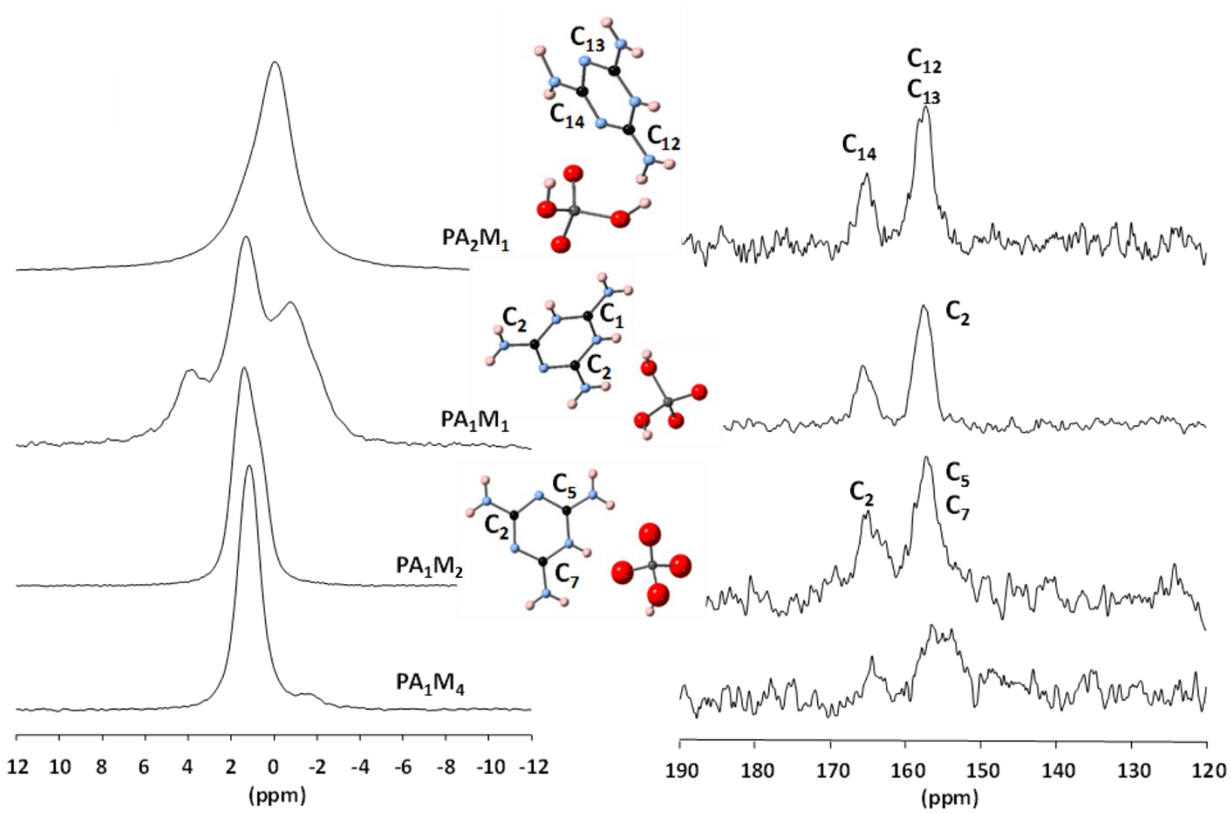

Fig. S4 (a) ^{31}P MAS and (b) ^{13}C CP MAS NMR spectra of PA_xM_y crystals. Assignment of the carbon signals is proposed according to NMR calculations on the crystalline structures.

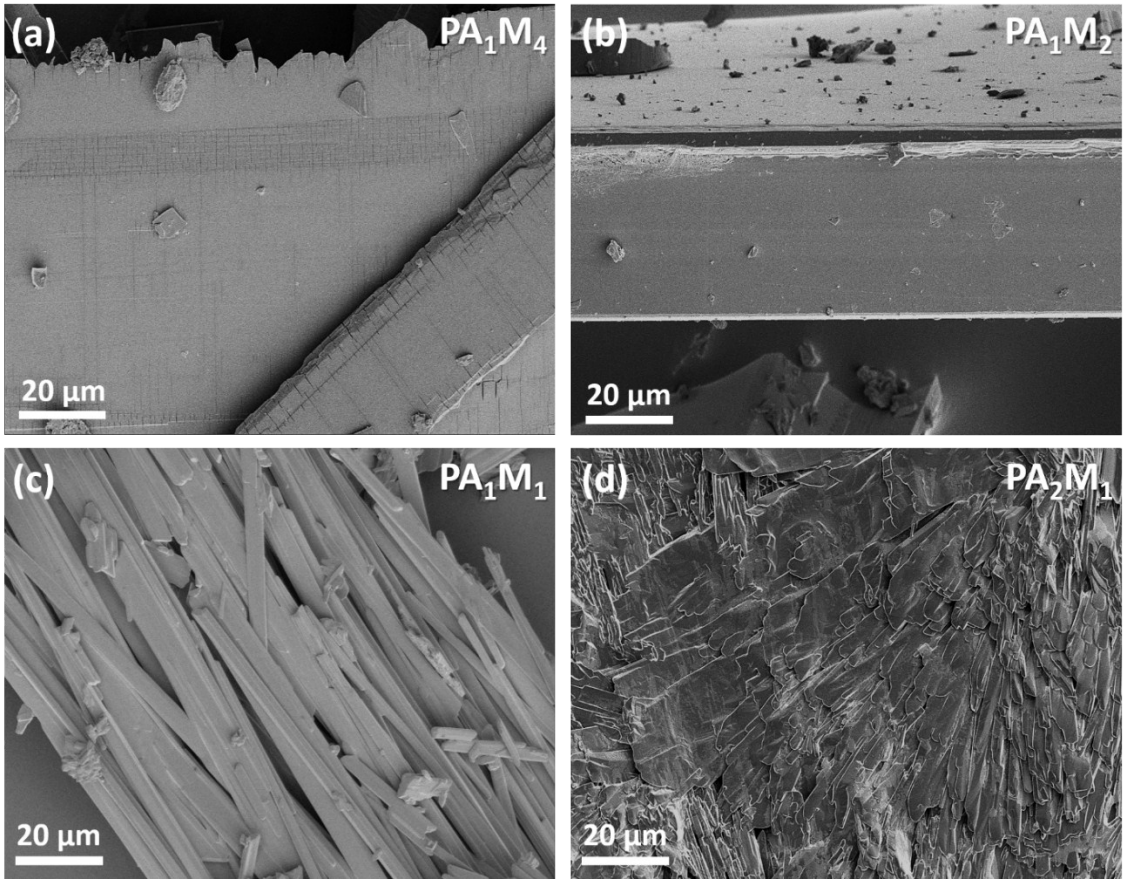

Fig. S5 SEM images of (a) PA_1M_4, (b) PA_1M_2, (c) PA_1M_1, and (d) PA_1M_1 crystals.

Table S3. EA and ICP data of PA_xM_y, which correspond to PA-M precursor molar ratio, melamine (M), and melamine single crystals (MSC) in wt. %.

Element	P	N	C	H	O
PA_2M_1	15.25	22.06	9.92	4.07	30.40
PA_1M_1	12.87	36.75	16.21	4.12	26.98
PA_1M_2	7.27	41.15	18.10	5.15	26.23
PA_1M_4	3.83	52.10	23.14	5.00	13.04
M	—	64.77	28.59	4.48	—
MSC	—	67.35	28.46	4.57	—

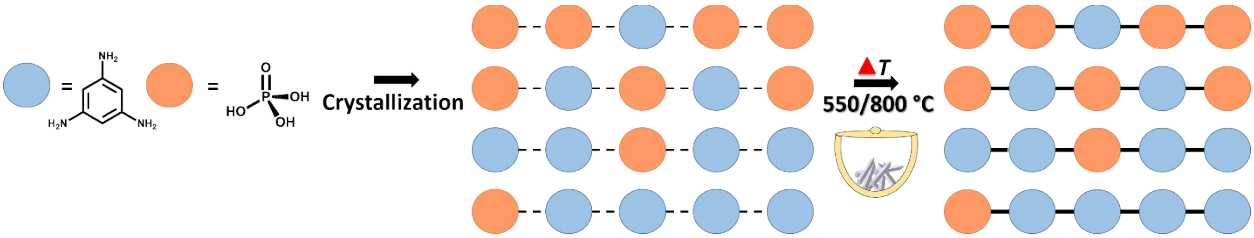

Fig. S6 General illustration of PNC_x materials synthesis.

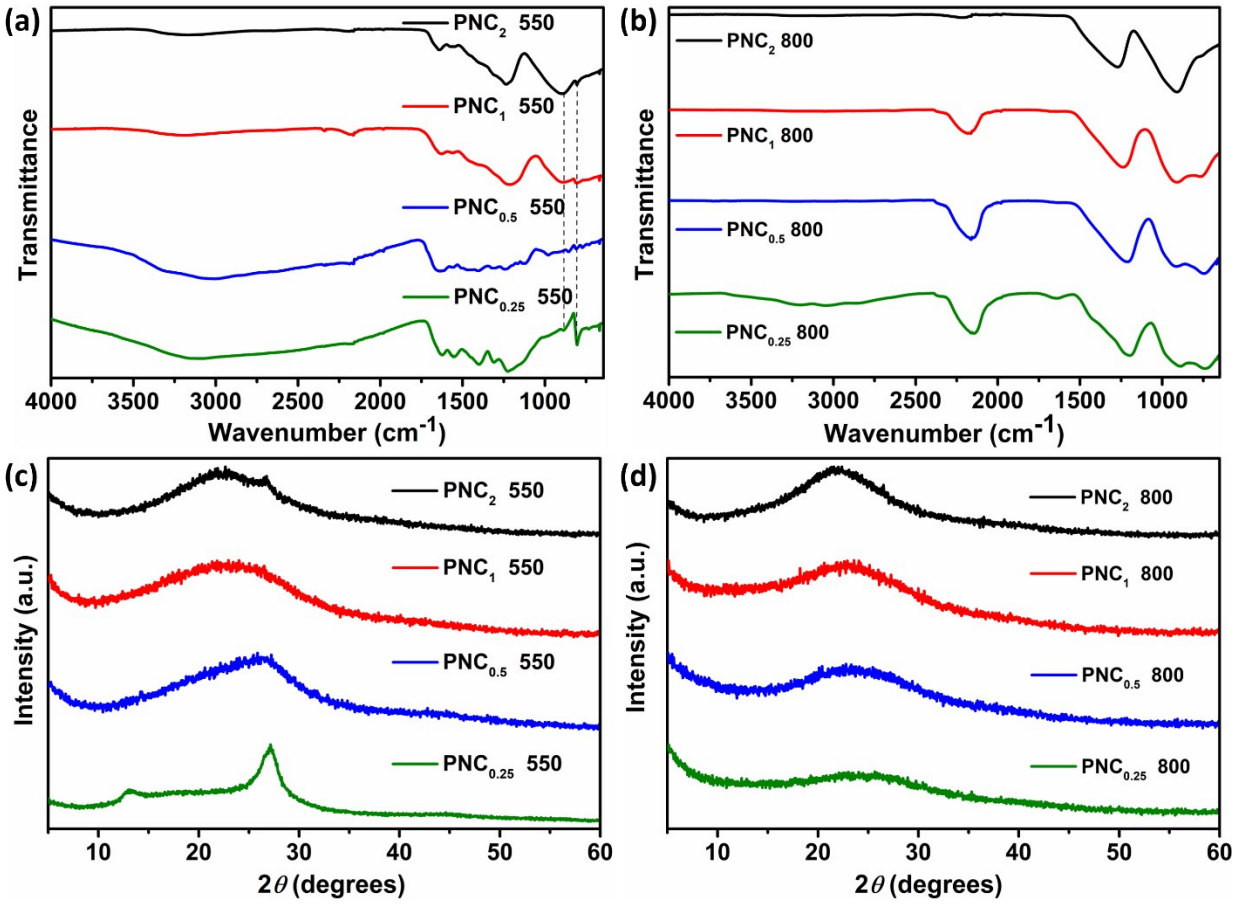

Fig. S7 FTIR spectra of (a) PNC_x 550 and (b) PNC_x 800. XRD patterns of (c) PNC_x 550 and (d) PNC_x 800. All spectra and patterns and are offset for clarity.

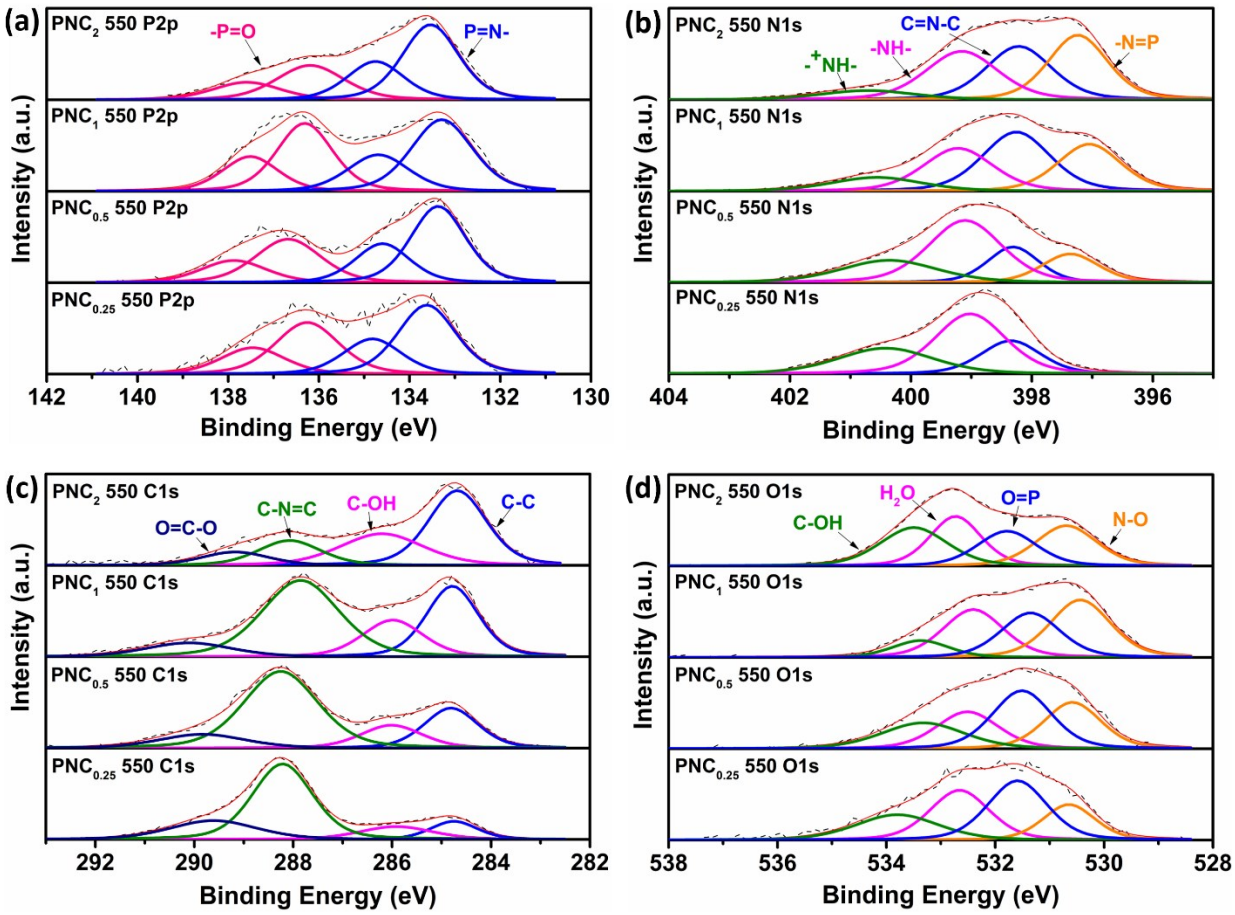

Fig. S8 PNC_x 550 XPS spectra for (a) $P2p_{3/2}$ and $P2p_{1/2}$, (b) N1s, (c) C1s, and (d) O1s.

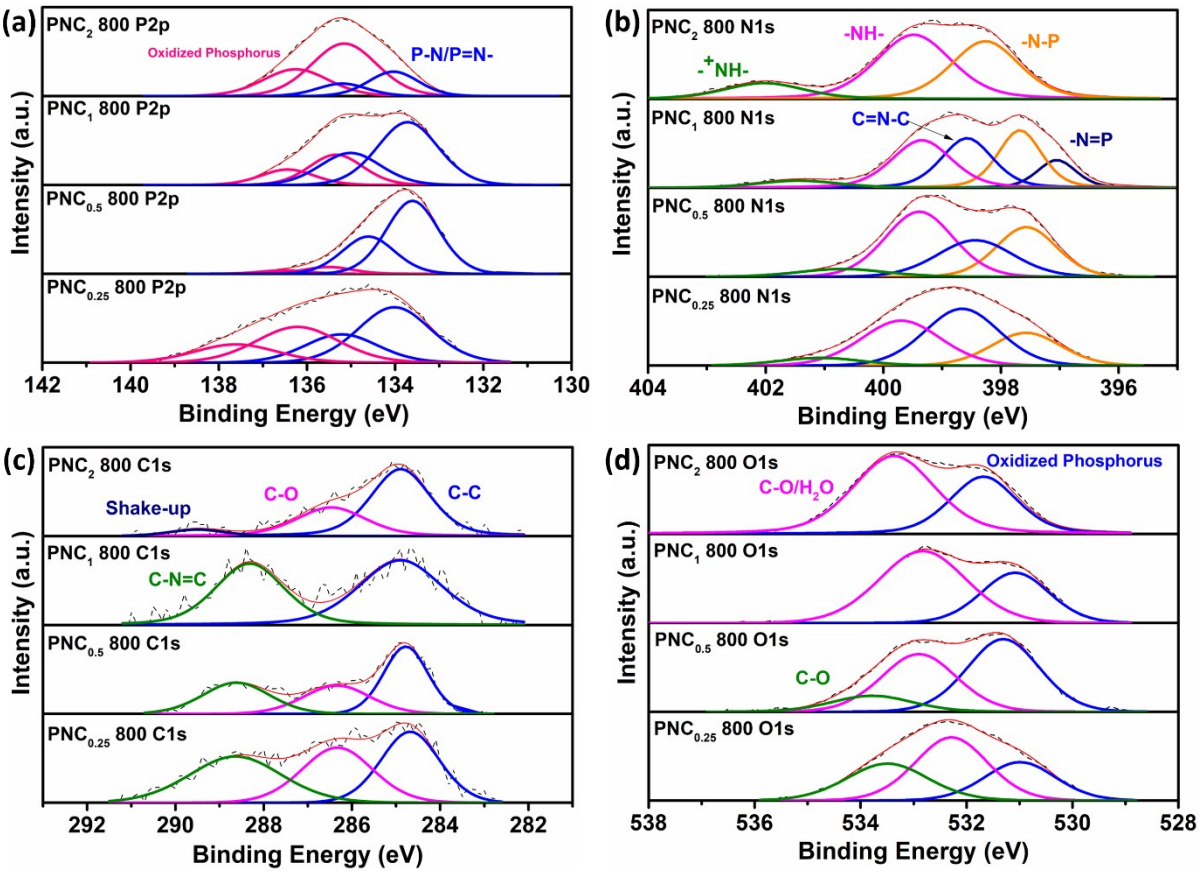

Fig. S9 PNC_x 800 XPS spectra for (a) $P2p_{3/2}$ and $P2p_{1/2}$, (b) N1s, (c) C1s, and (d) O1s.

The PNC_1 800 N1s spectrum expose five peaks at binding energies of: 397.0 (P=N), 397.7 (P-N), 398.6 (C-N=C), 399.4 (NH), and 401.5 eV (positively charged nitrogen atom).[5–8] The chemical contribution that belongs to the positively charged amine group, located at 402.3 eV in PNC_2 800, shifts to lower binding energies for lower *x* value due to larger amount of phosphanimine groups in the samples. Furthermore, the PNC_2 800 N1s spectrum shows only three nitrogen species at 397.5 (-N-P-), 398.9 (amine)[9], and 401.5 (-$^+$NH-) eV, suggesting the oxidation of the sp^2 C in C-N heterocycles. Both $PNC_{0.25}$ 800 and $PNC_{0.5}$ 800 C1s spectra show three species corresponding to C-C, C-O, and C-N=C chemical states, centered at 284.7, 286.3, and 288.6 eV, respectively.[10–12] PNC_1 800 presents only two chemical states attributed to C-C and C-N=C. The C1s spectrum of PNC_2 800 further confirms the low carbon content within the sample by the disappearance of the chemical state of C-N=C. Additionally, a new peak appears at 289.5 eV and may be caused by a shake-up π-π^* satellite.[13]

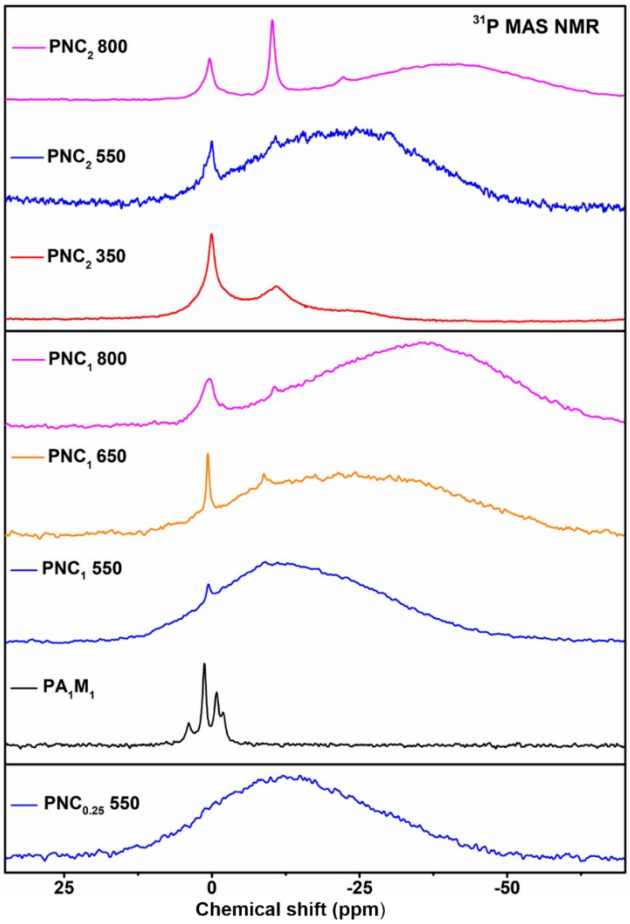

Fig. S10 ^{31}P MAS NMR of PA_1M_1 raw crystal (marked in black), PNC_2 calcined at 350 °C (marked in red), $PNC_{0.25}$, PNC_1, and PNC_2 calcined at 550 °C (marked in blue), PNC_1 calcined at 650 °C (marked in orange), and PNC_1, PNC_2 calcined at 800 °C (marked in magenta).

(a)

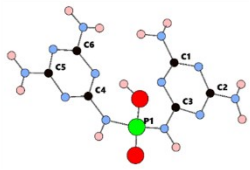

	δ (ppm)
P	-15,6
C1	169,0
C2	169,4
C3	167,0
C4	165,3
C5	166,7
C6	162,9

P
C
O
N
H

	δ (ppm)		δ (ppm)
P1	-11,7	C11	166,5
P2	-8,4	C12	167,4
P3	-30,1	C13	169,2
		C14	169,8
C1	168,5	C15	166,8
C2	170,5	C16	170,0
C3	172,9	C17	168,4
C4	166,5	C18	168,3
C5	168,8	C19	167,8
C6	168,1	C20	167,8
C7	167,3	C21	169,1
C8	170,5		
C9	168,4		
C10	165,6		

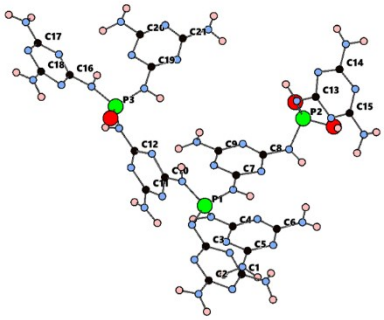

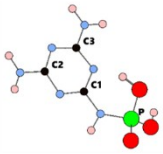

	δ (ppm)
P	-13,4
C1	164,4
C2	167,0
C3	162,9

(b)

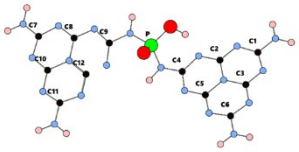

	δ (ppm)		δ (ppm)
P	-24,6	C6	166,3
		C7	166,4
C1	166,0	C8	158,3
C2	156,1	C9	166,5
C3	157,0	C10	157,7
C4	162,8	C11	166,5
C5	156,4	C12	158,0

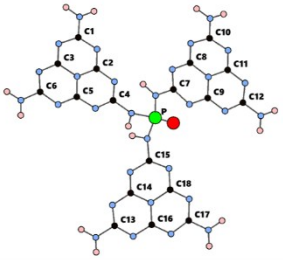

	δ (ppm)		δ (ppm)
P	-27,4		
C1	166,2	C10	166,6
C2	157,4	C11	158,2
C3	157,4	C12	166,4
C4	163,4	C13	167,0
C5	157,5	C14	158,9
C6	166,5	C15	168,7
C7	167,6	C16	158,3
C8	159,0	C17	166,4
C9	157,0	C18	158,4

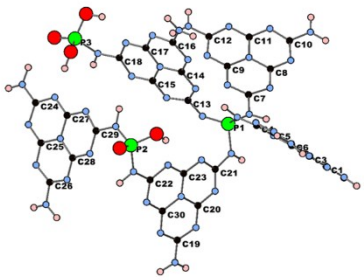

	δ (ppm)		δ (ppm)
P1	-28,2	C14	156,0
P2	-22,8	C15	157,2
P3	-1,9	C16	166,4
		C17	157,6
C1	166,5	C18	165,0
C2	158,1	C19	166,8
C3	157,3	C20	158,1
C4	165,2	C21	166,4
C5	157,9	C22	162,6
C6	166,6	C23	155,8
C7	167,6	C24	164,9
C8	158,7	C25	156,1
C9	157,4	C26	166,6
C10	166,3	C27	157,7
C11	157,9	C28	156,6
C12	166,6	C29	164,6
C13	169,2	C30	157,3

Fig. S11 Calculated ^{31}P and ^{13}C NMR parameters for a series of simple models with representative PO_xN_{4-x} environments with P linked to (a) melamine or (b) melem entities.

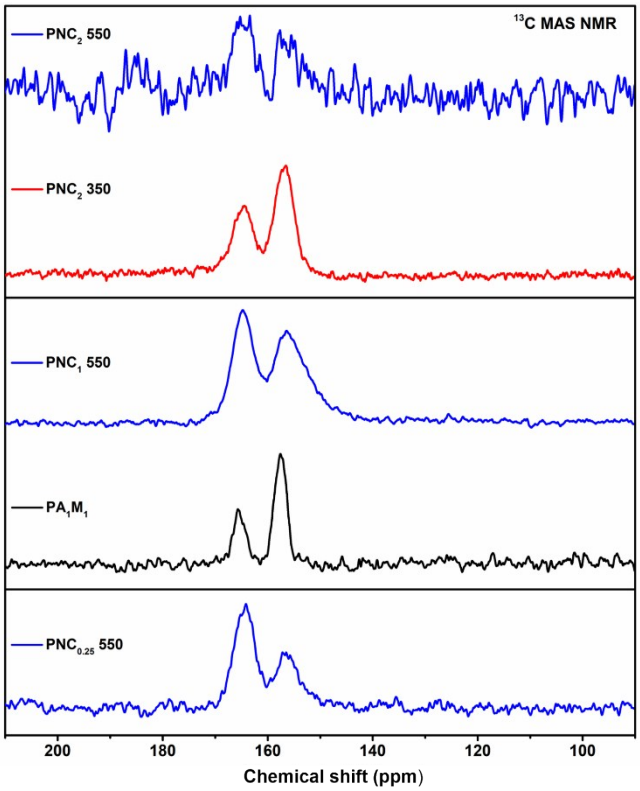

Fig. S12 ^{13}C CP MAS NMR spectra of PA_1M_1 crystal (marked in black), $PNC_{0.25}$, PNC_1, and PNC_2 synthesized at 550 °C (marked in blue), and PNC_2 synthesized at 350 °C (marked in red).

Table S4. EA and ICP of PNC_x (*x* is the PA:M molar ratio) calcined at 550 °C. All values are presented in wt. %.

Element	P	N	C	H	O
PNC_2 550	35.04	31.30	4.66	0.93	8.80
PNC_1 550	27.62	41.73	11.90	2.20	13.06
$PNC_{0.5}$ 550	16.74	48.04	21.69	1.61	7.43
$PNC_{0.25}$ 550	11.10	54.40	26.80	1.81	5.21

Table S5. EA and ICP of PNC_x (x is the PA:M molar ratio) calcined at 800 °C. All values are presented in wt. %.

Element	P	N	C	H	O
PNC_2 800	51.34	25.86	0.87	0.93	1.95
PNC_1 800	47.46	39.08	4.78	0.20	9.51
$PNC_{0.5}$ 800	48.47	40.58	5.46	0.25	4.81
$PNC_{0.25}$ 800	43.34	32.81	5.30	0.73	8.19

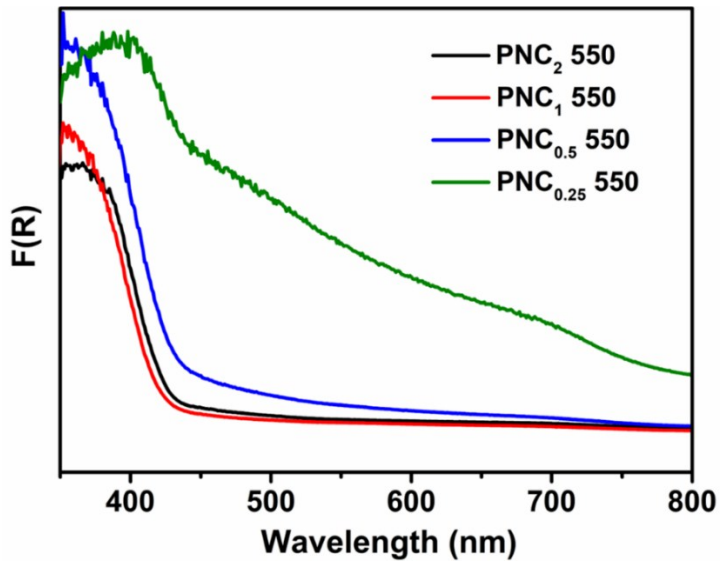

Fig. S13 PNC_x 550 UV-vis spectra. F(R) is Kubelka-Munk function that represents absorbance based on a reflectance measurement.

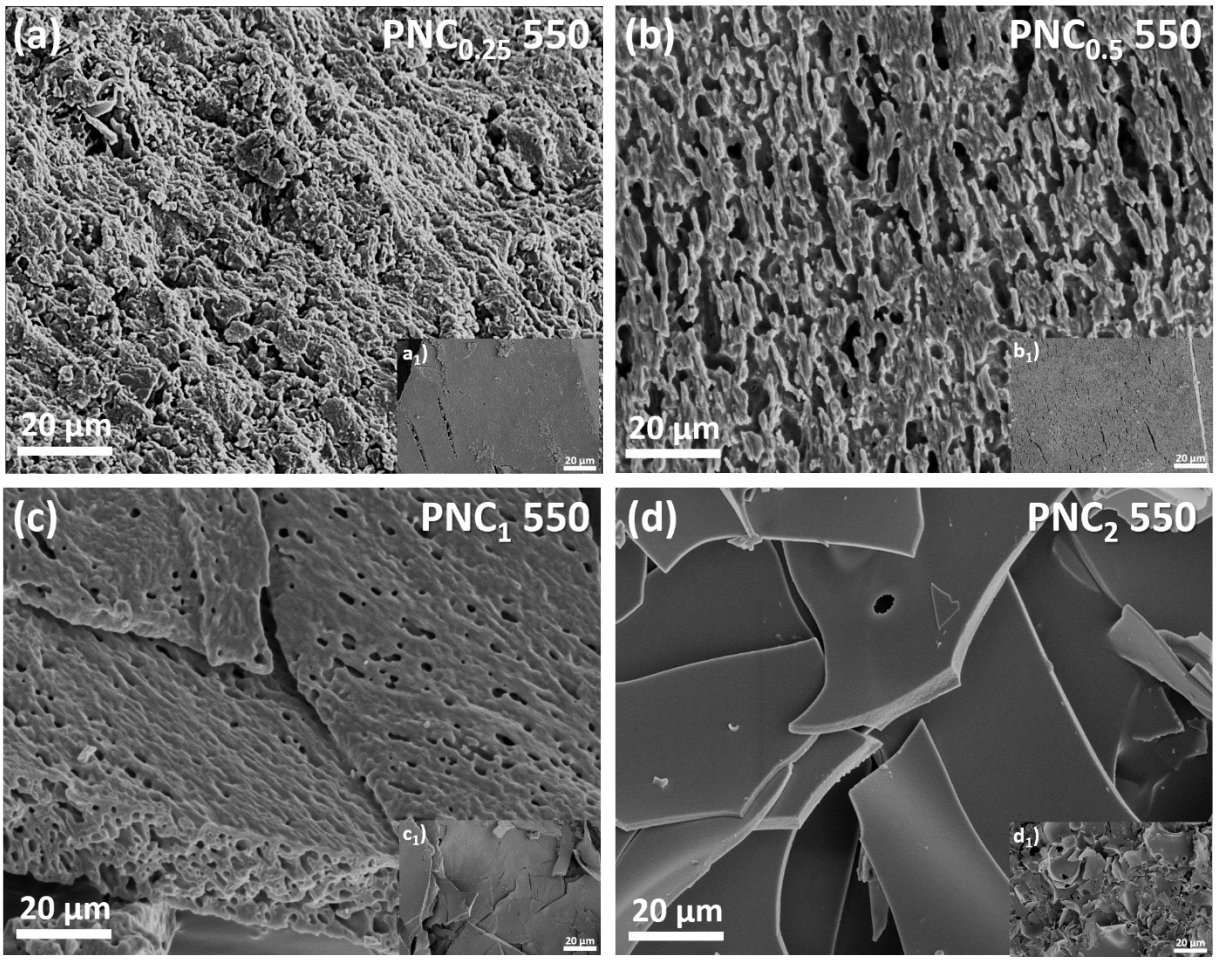

Fig. S14 SEM images of PNC_x 550 materials.

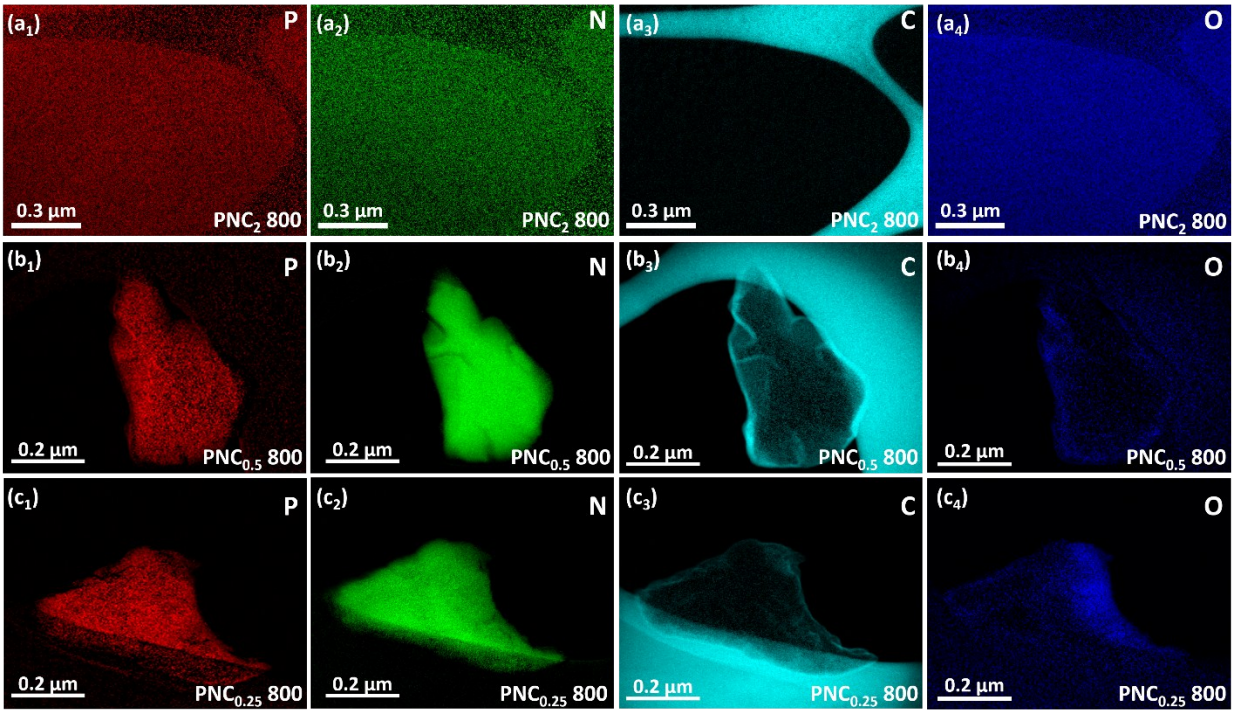

Fig. S15 EFTEM of (a_x) PNC_2 800, (b_x) $PNC_{0.5}$ 800 and (c_x) $PNC_{0.25}$ 800 (x = 1, 2, 3, 4 for phosphorus, nitrogen, carbon, and oxygen, respectively) supported on an ultrathin carbon grid.

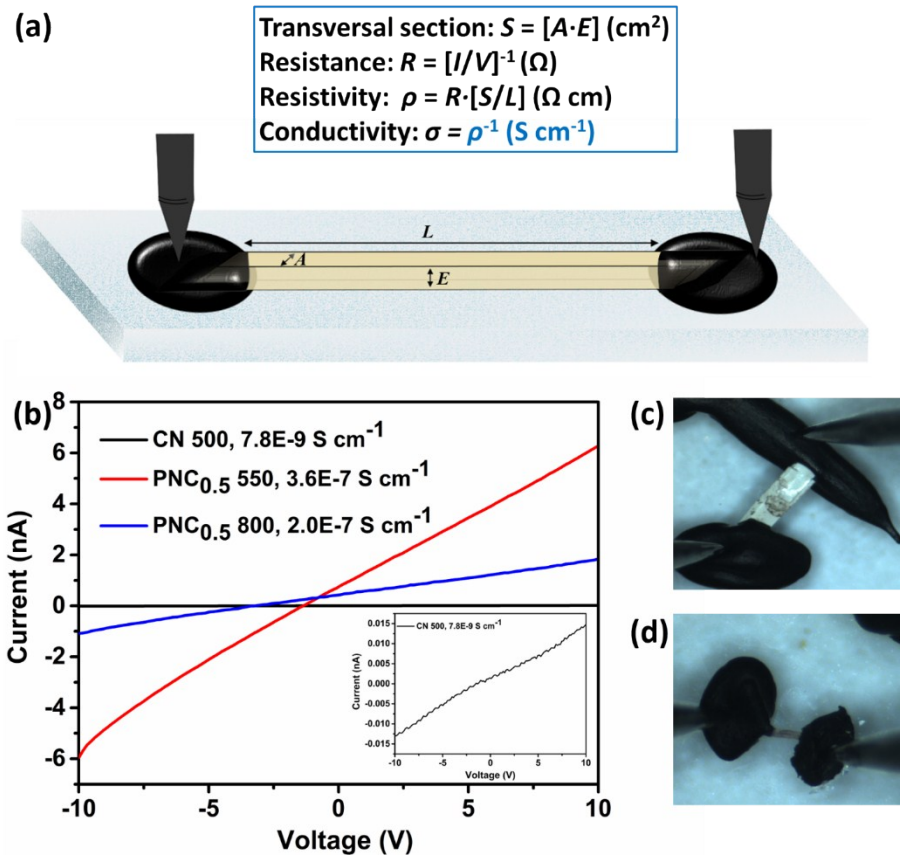

Fig. S16 Electrical conductivity measurements. a) Illustration of electrical conductivity measurement setup, (b) *I–V* plots of $PNC_{0.5}$ 550, $PNC_{0.5}$ 800, optical images of (c) $PNC_{0.5}$ 550, and (d) $PNC_{0.5}$ 800 while placing between two conductive tungsten probes. Calculated conductivity values: σ(CN 500) = 7.8×10^{-9} S cm^{-1}, σ($PNC_{0.5}$ 550) = 3.6×10^{-7} S cm^{-1}, and σ($PNC_{0.5}$ 800) = 2.0×10^{-7} S cm^{-1}.

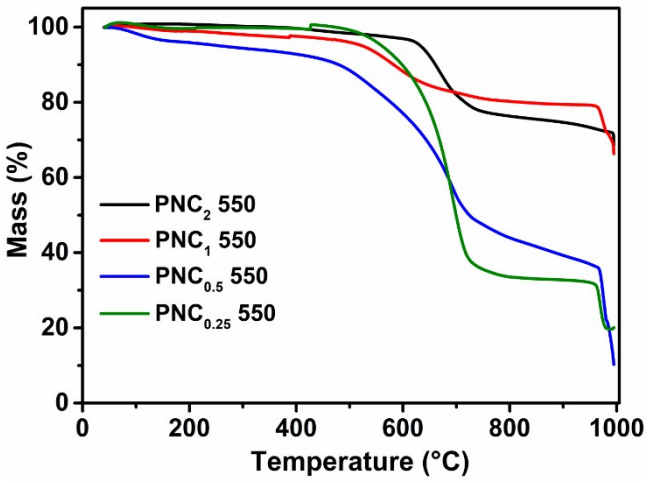

Fig. S17 Thermal gravimetric analysis (TGA) curves of PNC_x 550 under air.

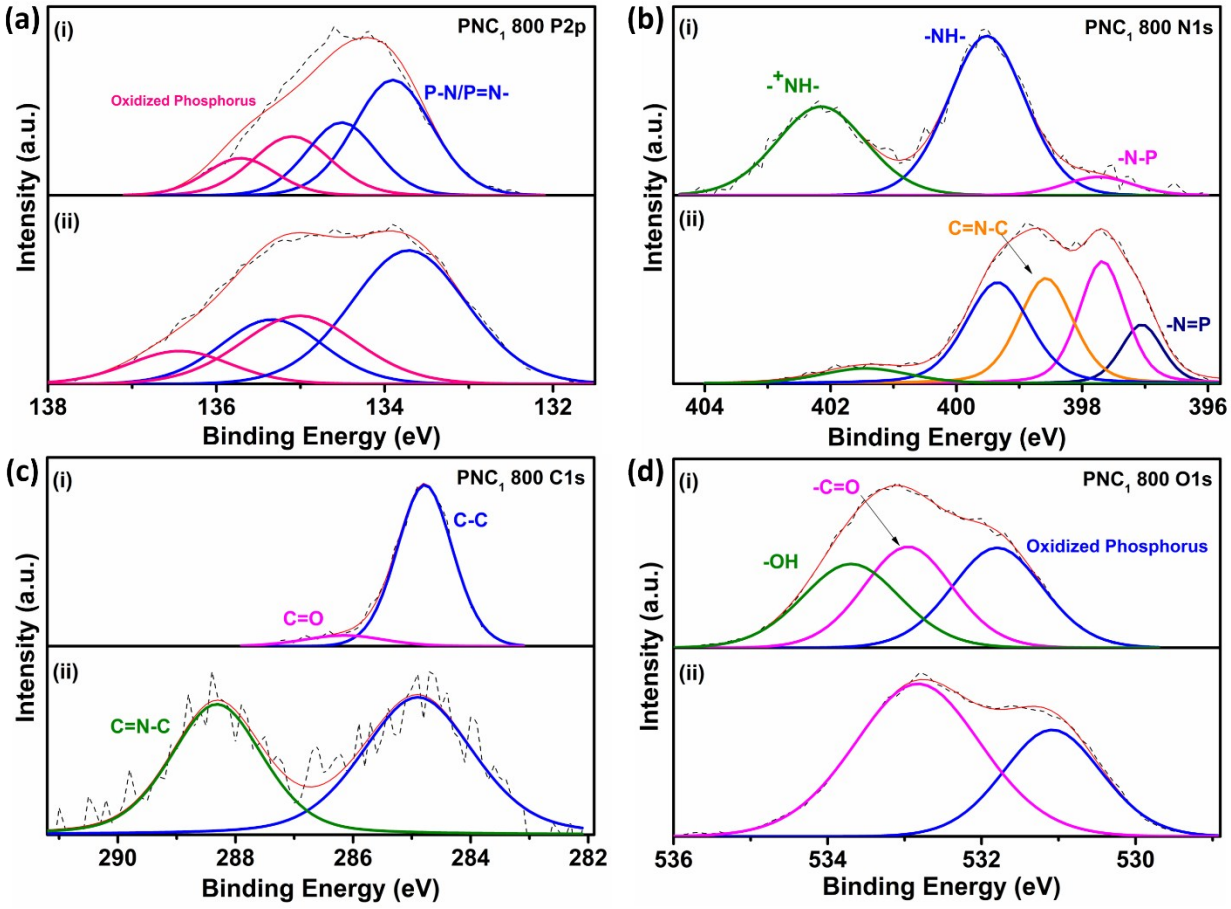

Fig. S18 PNC_1 800 XPS spectra for (a) P2p, (b) N1s, (c) C1s, and (d) O1s: after (i) and before (ii) burning under visible fire.

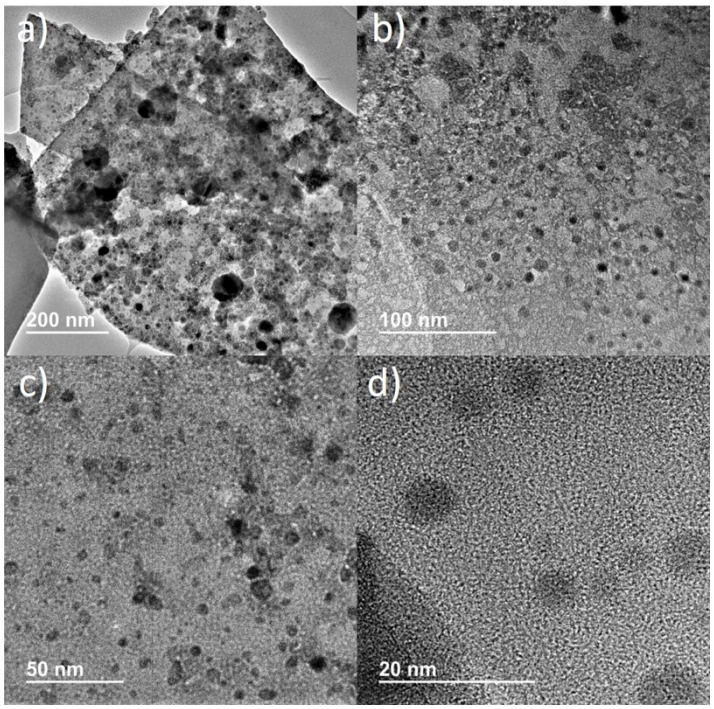

Fig. S19 HRTEM images of Ni/PNC$_{0.5}$ 800 at different magnifications.

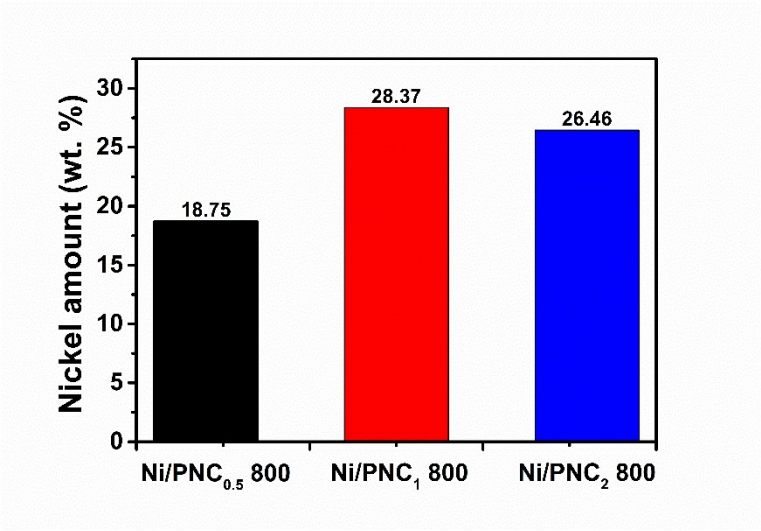

Fig. S20 Ni/PNC$_x$ 800 nickel content in weight percentage (measeured using ICP-OES).

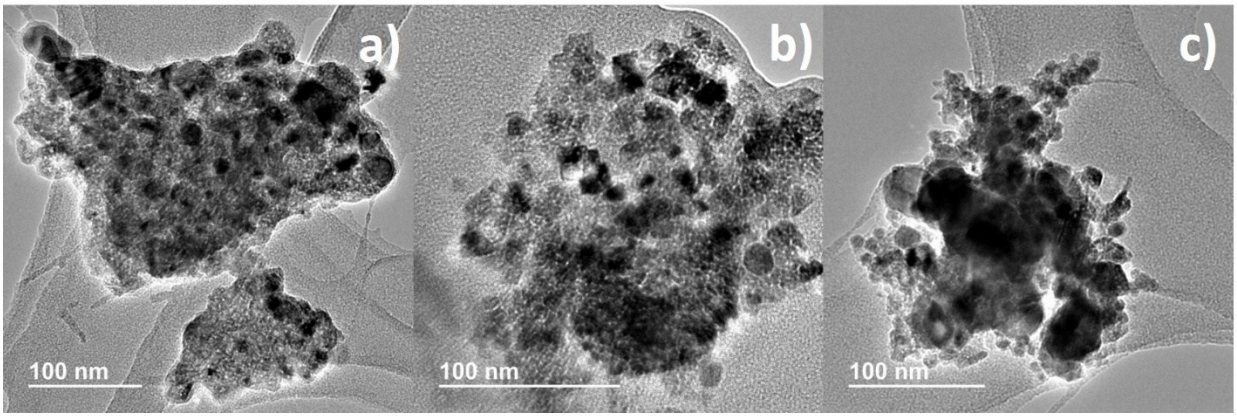

Fig. S21 HRTEM images of $Ni/PNC_{0.5}$ (a), Ni/PNC_1 (b), and Ni/PNC_2 (c) after 20 h methanation reaction at 400 °C.

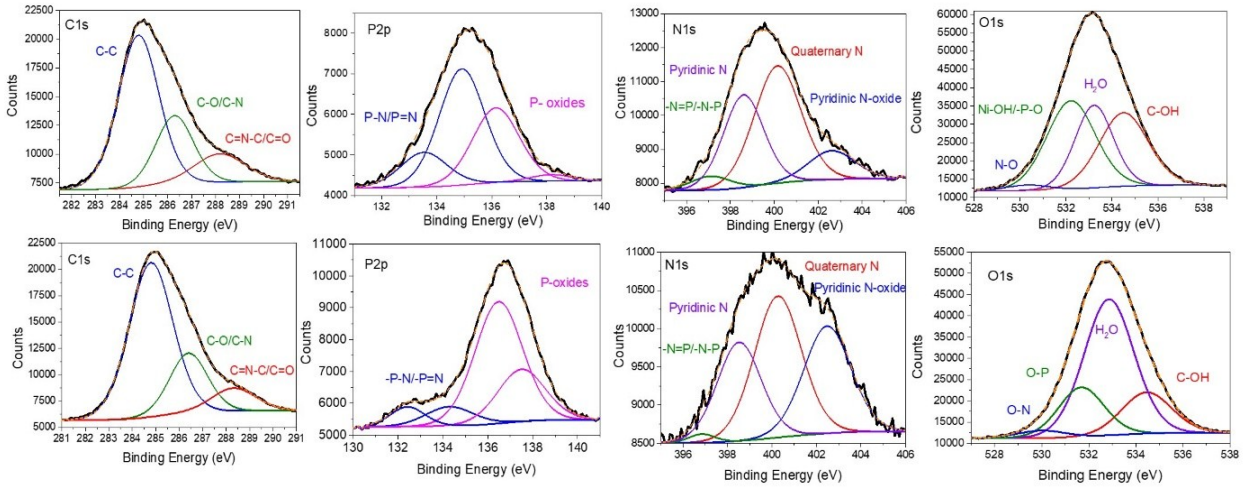

Fig. S22 XPS of $PNC_{0.5}$ 800 before (top panels) and after reaction (bottom panels).

References

1 D. J. A. De Ridder, K. Goubitz, V. Brodski, R. Peschar and H. Schenk, *Helv. Chim. Acta*, 2004, **87**, 1894–1905.

2 X. Li, S. Feng, F. Wang, Q. Ma and M.-L. Zhu, *Acta Crystallogr. Sect. E Struct. Reports Online*, 2010, **66**, o239–o240.

3 S. T. Huang, G. L. Wang, N. B. Li and H. Q. Luo, *RSC Adv.*, 2012, **2**, 10948–10954.

4 P. Li, H. D. Arman, H. Wang, L. Weng, K. Alfooty, R. F. Angawi and B. Chen, *Cryst. Growth Des.*, 2015, **15**, 1871–1875.

5 A. Fukushima, A. Hayashi, H. Yamamura and M. Tatsumisago, *Solid State Ionics*, 2017, **304**, 85–89.

6 J. Wu, S. Yang, J. Li, Y. Yang, G. Wang, X. Bu, P. He, J. Sun, J. Yang, Y. Deng, G. Ding and X. Xie, *Adv. Opt. Mater.*, 2016, **4**, 2095–2101.

7 W. Liang, J. Lei and C. R. Martin, *Synth. Met.*, 1992, **52**, 227–239.

8 M. L. Kantam, M. Roy, S. Roy, B. Sreedhar and R. Lal De, *Catal. Commun.*, 2008, **9**, 2226–2230.

9 J. Yue and A. J. Epstein, *Macromolecules*, 1991, **24**, 4441–4445.

10 P. Goli, S. Legedza, A. Dhar, R. Salgado, J. Renteria and A. A. Balandin, *J. Power Sources*, 2014, **248**, 37–43.

11 G. Wulff, H. Schmidt and L. Zhu, *Macromol. Chem. Phys.*, 1999, **200**, 774–782.

12 J. Xu, L. Zhang, R. Shi and Y. Zhu, *J. Mater. Chem. A*, 2013, **1**, 14766.

13 L. Tao, Q. Wang, S. Dou, Z. Ma, J. Huo, S. Wang and L. Dai, *Chem. Commun.*, 2016, **52**, 2764–2767.